International Journal of Refractory Metals and Hard Materials 108 (2022) 105949

Contents lists available at ScienceDirect

International Journal of Refractory Metals and Hard Materials

journal homepage: www.elsevier.com/locate/IJRMHM

Assessment of fracture toughness of cemented carbides by using a shallow notch produced by ultrashort pulsed laser ablation, and a comparative study with tests employing precracked specimens

L. Ortiz-Membrado [a], C. Liu [b], J. Prada-Rodrigo [c], E. Jiménez-Piqué [a,d], L.L. Lin [e], P. Moreno [c], M.S. Wang [e], L. Llanes [a,d,*]

[a] CIEFMA, Department of Materials Science and Engineering, Universitat Politècnica de Catalunya - BarcelonaTech, Campus Diagonal Besòs-EEBE, 08019 Barcelona, Spain
[b] Xiamen Tungsten Co., Ltd., 361009 Xiamen, China
[c] ALF-USAL, Research Group in Laser Applications and Photonics, Universidad de Salamanca, 37008 Salamanca, Spain
[d] Barcelona Research Center in Multiscale Science and Engineering, Universitat Politècnica de Catalunya - BarcelonaTech, Campus Diagonal Besòs, 08019 Barcelona, Spain
[e] Xiamen Golden Egret Special Alloy Co., Ltd., 361006 Xiamen, China

ARTICLE INFO

Keywords:
Fracture toughness
Ultrashort pulsed laser ablation
Surface "through-thickness" micronotches
Cemented carbides

ABSTRACT

The use of fracture mechanics for rationalizing the fracture behavior of cemented carbides is valid, as far as sharp cracks, free of residual stresses and subjected to a well-defined stress state are used for assessing fracture toughness. However, machining a very sharp notch on the surface of hardmetals for fracture toughness testing has been a critical issue during many years. Within this context, introduction of surface "through-thickness" micronotches (SEμVNB) by means of ultrashort pulsed laser ablation (UPLA) is here proposed, implemented and analyzed as an innovative precracking-like route within flexural testing procedures for appropiated evaluation of fracture toughness of cemented carbides. UPLA parameters used for introducing the micronotch are optimized in terms of induced damage ahead of the notch tip. For comparison purposes, fracture toughness is also determined by means of flexural testing of previously cracked single-edge notch beams (SENB-Cracked) as well as specimens with V-notch tips sharpened through diamond polishing using a razor blade, and Palmqvist indentation microfracture method. The satisfactory agreement found between values measured using UPLA-micronotched and SENB-Cracked (reference) specimens allows to conclude that flexural testing of SEμVNB samples is a valid methodology for reliable determination of fracture toughness of hardmetals. This is feasible because of the extremely short time of laser-matter interaction. It yields small and somehow controlled damage in front of the notch tip as a result of shock wave propagation during ablation, which translates into effective precracking of SEμVNB specimens.

1. Introduction

Cemented carbides based upon tungsten carbide, materials usually referred to as hardmetals, have been increasingly used since their invention, about one century ago [1]. Historically, this evolution has mainly taken place on the basis of replacement of steels as cutting tools due to their higher hardness and improved wear resistance at high temperatures, generally at some expense of fracture toughness [2]. However, the range of applications for hardmetals is getting wider. In this regard, although their intrinsic hard nature is always an attribute, some of their existing as well as most of their emerging and/or consolidating applications require a higher relevance of toughness for enhancing material performance and reliability of tools and components. Hence, from the perspective of optimizing microstructural design of cemented carbides, reliable and cost-effective evaluation of fracture toughness is a continuously demanded action.

Definition and measurement of fracture toughness of hardmetals has always been a challenging subject. Regarding terminology, it adopted

* Corresponding author at: CIEFMA, Department of Materials Science and Engineering, Universitat Politècnica de Catalunya - BarcelonaTech, Campus Diagonal Besòs-EEBE, 08019 Barcelona, Spain.
E-mail address: luis.miguel.llanes@upc.edu (L. Llanes).

https://doi.org/10.1016/j.ijrmhm.2022.105949
Received 23 March 2022; Received in revised form 5 July 2022; Accepted 10 July 2022
Available online 12 July 2022
0263-4368/© 2022 Elsevier Ltd. All rights reserved.

(and still does) different meanings throughout the years: transverse rupture strength of an unnotched specimen subjected to flexural testing, energy absorbed during fracture of a notched sample tested under dynamic/impact loading conditions, work required for nucleation and extension of cracks out of imprints resulting from sharp indentation, and finally critical stress intensity factor for crack extension (K_{Ic}) using a precracked specimen [3,4]. The latter, K_{Ic}, is directly linked to the advent of fracture mechanics application to cemented carbides – about half a century ago [5] -, and has allowed to partly overcome specific drawbacks already indicated by Kenny at that time: sensitivity to surface finish of specimens employed, degree of scatter of attained results and, maybe the most important, the generic empirical nature of toughness as a mechanical parameter. However, use of K_{Ic} for defining fracture toughness does not solve the referred issue by itself, as its effective and reliable implementation requires the suitability for introducing crack-like features in these hard and brittle-like materials, amenable to a direct and unambiguous characterization of subsequent tensile fracture using available fracture mechanics methods [6]. Within this context, the employment of methods using either chevron-notched samples or notched/precracked ones are usually invoked for defining baseline (reference) values, against which compare the ones measured by employing other testing protocols (e.g. Refs. [7–14]). This is particularly relevant for assessment of accuracy and reliability of reported toughness values. In this regard, it should be highlighted that, although indentation fracture toughness (IFT) testing is the most simple, cost-effective and widespreadly used method [15], it is well-established that values determined by IFT are overestimated for grades whose hardness is lower than 1300–1400 HV30, and corresponding discrepancies increase with rising binder content and carbide grain size [13,16]. Meanwhile, it is also known that testing protocols involving notched/precracked specimens imply relevant challenges in machining/shaping the required geometries as well as special equipment needed for final fracture testing [3,4,17]. Hence, there has always been a continuous search for alternative notching and precracking approaches.

Following above ideas, ultrashort pulsed laser ablation (UPLA) emerges as an interesting option, as it has shown potential for post-processing and fabrication as well as surface texturing of hardmetal tools and components (e.g. Refs. [18–29]). Main reason behind it is that UPLA involves an extremely short interaction time with the target material; thus, the latter is removed involving minimum heat transfer to the remaining substrate. As a result, not only precise dimensions and geometry are attained, but also microstructural changes and thermal damage are effectively diminished [30–32]. Recent research by groups involved in this study has shown that notch micromachining by means of UPLA is a suitable technique for accurate and reliable measurement of fracture toughness in several fine-grained ceramics, i.e. yttria- and ceria-stabilized zirconia as well as silicon nitride, using single-edge V-notch specimens [33–36]. Successful implementation of this machining approach is related to the possibility of introducing very short and sharp notches where a micro-damaged zone is generated in front of the notch tip. Within this framework, it is the main objective of this work to evaluate the suitability of shallow through-thickness micronotches, introduced by UPLA in bending bars, for evaluating the fracture toughness of three hardmetal grades. Investigation includes an initial optimization of laser ablation parameters in terms of induced damage. Accuracy and reliability of the results found are then assessed by direct comparison of them with fracture toughness baseline values, measured using single-edge notched beams where a precrack is first introduced by cyclic compression under reverse bending. Furthermore, for comparison purposes, values determined by means of indentation fracture toughness are also reported. Finally, mechanical testing results are complemented by extensive and detailed fractographic inspection of broken surfaces. In doing so, special attention is paid to document fracture micromechanisms operative at damaged or precracked regions, as compared to those related to unstable crack propagation.

2. Experimental aspects

2.1. Materials studied

The study is conducted in three microstructurally different WC-Co grades. Binder content has been defined as experimental variable, whereas carbide grain size has been held fixed. Hardmetal grades studied are here referred to as U10, U20 and U25.

Single-phase microstructural parameters determined in this investigation refer to binder weight content ($\%_{wt.}$ *binder*) and carbide mean grain size (d_{WC}). They were determined from information gathered from direct observation by means of Field Emission Scanning Electron Microscopy (FESEM), including the use of Energy Dispersive X-Ray Analysis (EDX), using a Jeol JSM-7001F unit. Prior to FESEM inspection, samples were ground and diamond polished up to mirror-like surface finish following a 6, 3 and 1 μm sequence, with a final colloidal silica stage. Carbide mean grain size was measured following the linear intercept method in FESEM micrographs. Hardness was determined by indenting polished surfaces with an applied load of 30 Kgf (294 N) and using a diamond Vickers indenter. Representative images of microstructural assemblage of studied materials, as well as results from this basic microstructural and mechanical characterization are given in Fig. 1 and Table 1 respectively.

2.2. Fracture toughness assessment

Fracture toughness of specimens with shallow and through-thickness UPLAed notches was determined by the Single Edge V-Notch Beam (SEVNB) method. As it will be seen later, use of this machining route allows to effectively get V-micronotches with depth of several tens of microns and tip width of just a few microns. Accordingly, testing and results where the use of these specimens is involved are tagged in this study as SEμVNB. Detailed information on UPLA parameters is given in Section 3.1. Three V-micronotched samples per grade, with 45x5x4 mm dimensions, were tested to failure in a servohydraulic mechanical testing machine (Instron, Model 1341), using a four-point bending test configuration with spans of 40/20 mm, and at constant loading rates between 200 and 400 N/s. Aiming to compare the value of K_{Ic} obtained by using the SEμVNB technique, fracture toughness was also measured by using the single-edge notch beam (SENB) method, but using effectively precracked specimens. Detailed information on precracking procedure is given in Section 3.2. As in the case of SEμVNB samples, fracture toughness was determined by testing six notched specimens per grade, in this case with 45x10x5 mm dimensions, to failure under similar loading conditions. In doing so, different notch/crack configurations were used, as it will be described in Section 3.2. The stress intensity factor, K_I, for all notched specimens was obtained by using the following expression [37]:

$$K_I = \sigma Y \sqrt{a} \tag{1}$$

$$Y = \frac{1.1215\sqrt{\pi}}{\beta^{3/2}} \times \left[\frac{5}{8} - \frac{5}{12}\alpha + \frac{1}{8}\alpha^2\beta^6 + \frac{3}{8}exp\left(-\frac{6.1342\alpha}{\beta}\right)\right] \tag{2}$$

where a is the crack length, Y is a geometry factor that depends on the configuration of the sample with the notch and the manner in which the loads are applied, $\alpha = a/W$ and $\beta = (1-\alpha)$.

Finally, fracture toughness was evaluated, for comparison purposes too, by using the IFT method. It was done by measuring the length of arrested cracks, emanating from the corners of Vickers indentation under applied load of 294 N, and relating it to fracture toughness of the material via the relationship proposed by Shetty et al. [16], according to:

$$K_{Ic} = \beta \cdot \sqrt{HV \cdot \frac{P}{4L}} \tag{3}$$

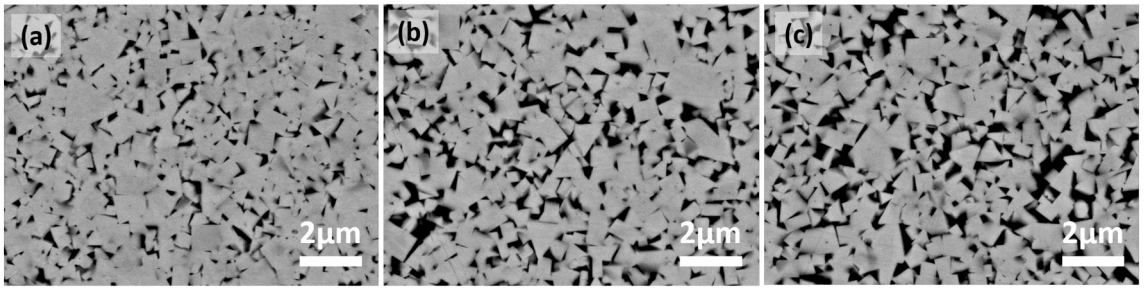

Fig. 1. FESEM micrographs of investigated cemented carbide grades: **(a)** U10, **(b)** U20, and **(c)** U25.

Table 1
Metallic binder content, carbide mean grain size and hardness for the hardmetal grades studied.

Grade	$\%_{wt.}$ binder*	d_{WC} (µm)	HV30
U10	5.9 Co	0.63	1840
U20	9.6 Co	0.67	1620
U25	11.0 Co	0.72	1540

* All samples contain a small amount (about 0.5%wt.) of Cr_3C_2.

where HV is the hardness (N/mm^2), P is the applied load (N), L is the average of the length of the cracks at the imprint corners (mm), β is an empirical constant with value of 0.0889, and K_{Ic} is given as MPa $m^{1/2}$.

3. Results and discussion

3.1. Optimization of laser ablation parameters for shaping shallow notches in cemented carbides

For each hardmetal grade, 18 "through-thickness" notches (separated by about 300 µm from each other), were shaped. They were generated by inducing material ablation as a result of tight focusing of ultrashort laser pulses, delivered by a system based on the chirped pulsed amplification technique. Equipment used is composed of a Ti: Sapphire oscillator (Mai Tai, Spectra Physics) and a regenerative amplifier system (Spitfire Ace, Spectra Physics). Pulses had the following features: 60 fs of duration; 795 nm of wavelength, and 5 kHz of repetition rate. The pulse energy, together with the scanning speed and the number of passes, were the key parameters to optimize laser ablation in terms of induced damage. The samples were placed on a XYZ motorized stage and moved along one of the horizontal axis with different scanning speeds. To attain the desired notch depth (between 10 and 40 µm) multiple pass strategy was required. In this case, to check UPLA performance on the materials under consideration, the following parameters were used: pulse energy (µJ), with values between 1.5 and 4.0; scanning speed (µm/s), with values between 250 and 750; and number of passes, with values between 2 and 4. After combined and complementary optical and FESEM inspection of all the machined notches, optimized laser-ablation conditions were selected on the basis of well-defined notch sharpness and appropriated depth without excessive induced damage at the notch tip (e.g. Fig. 2). They were pulse energy of 4.0 µJ; scanning speed of 500 µm/s; and number of passes of 4. Once these parameters were defined, a single through-thickness notch was laser ablated in each specimen. It was placed within the span of 20 mm where maximum tensile stresses are imposed at the surface during flexural testing in four-point bending. Detailed analysis and measurement of notch and affected zone (at the notch tip) was conducted by FESEM before and after mechanical testing. As indicated above, these specimens are referred to as SEµVNB in this study.

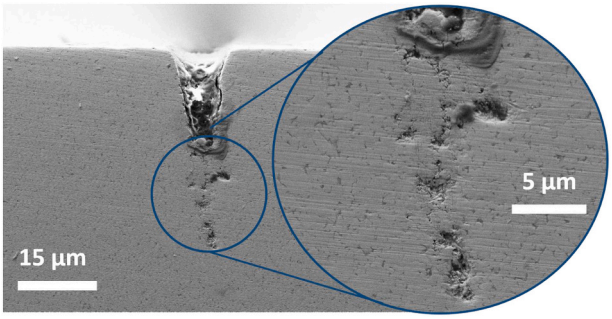

Fig. 2. FESEM micrograph of section of UPLAed notch, shaped using optimized laser parameters (i.e. SEµVNB specimen). Some damage in front of the notch tip as a result of shock wave propagation during ablation is observed, as it has been previously reported in other materials following the same machining process [33–36].

3.2. Notch sharpening, precracking and relief of induced residual stresses in cemented carbides

Accurate and reliable assessment of fracture toughness requires specimens containing sharp cracks, free of residual stresses. However, this is not an easy task to achieve in hard/brittle materials. Within this context, different notched/cracked specimens were used.

Six samples per hardmetal grade were first notched by electrical discharge machining, with a length-to-specimen width ratio of 0.3. In all of them, the notch tip was first sharpened by polishing the notch root with a razor blade impregnated with diamond paste, until a final width as low as 40–80 µm was reached (e.g. Fig. 3). This yielded a SEVNB geometry similar to the one described in the previous section, but involving deeper notches with less sharp tips than those shaped in SEµVNB specimens. Two specimens per each material studied were tested to failure using this configuration, and they are simply tagged as

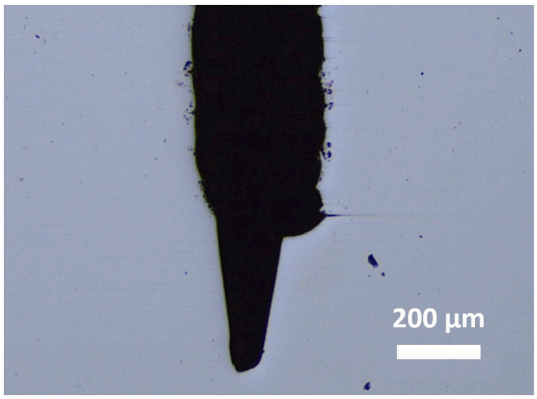

Fig. 3. Optical microscopy image showing notch aspect of a sharpened V-tip SENB geometry (i.e. SEVNB specimen).

SEVNB.

A sharp precrack was induced by compressive cyclic loads [6,8,9,11] in remnant V-tip and notched specimens. It was conducted under reverse cyclic bending [38–40], and the loading conditions used during the precracking procedure included: sine waveform, load ratio (R) of 10, testing frequency of 15 Hz and maximum (nominal) compressive stress of about 600–900 MPa at the upper side, where the notch was located. The sides of SENB specimens were polished to discern crack emergence using a high-resolution confocal microscope. Nucleation of small but well-defined cracks (e.g. Fig. 4) was observed after a number of cycles ranging from 10^4 to 10^5 cycles, depending on the value of compressive stresses applied.

It is known that residual stresses may be induced during cyclic compression precracking of notched samples [8,9,11]. Hence, all notched and precracked specimens were subjected to tensile fatigue, aiming to further propagate the small cracks induced during cyclic compression (e.g. Fig. 5a). Such subcritical crack growth was conducted under far-field cyclic tensile loads (R value of 0.1) in four-point bending and a test frequency ranging from 0.5 to 10 Hz. Crack extension behavior under constant applied load ranges was also monitored. For applied load values ranging from 650 to 900 N (corresponding to nominally applied stress intensity factor values between 4 and 6 MPa$\sqrt{m}$), cracks were observed to grow at decreasing rates, until total arrest was attained (e.g. Fig. 5b). For applied maximum loads higher than 980 N and previous crack extensions of about 200–300 μm (Fig. 5b), an accelerated crack growth behavior was discerned, indicating crack propagation through regions free of residual stress influence [8,9]. At that stage, specimens with extended precracks were tested to rupture, and they are tagged here as SENB-Cracked.

All broken specimens were fractographically inspected by means of FESEM (Zeiss Neon 40). In doing so, special attention was paid to observe transitions in both fracture scenario and failure micromechanisms involved as the crack front was stably extending from the notch tip until unstable failure was triggered.

3.3. *Fracture toughness assessment, fractographic inspection and critical comparison of the results attained using different testing methods*

Experimentally measured values of fracture toughness are listed in Table 2. It includes results determined using specimens with distinct notch/crack configurations: (1) V-micronotches shaped by USP laser ablation [SEμVNB]; (2) nucleated and extended precracks, out of the existing notch by means of cyclic compression followed by stable growth under cyclic tensile bending [SENB-Cracked]; and (3) V-notch tips sharpened through diamond polishing [SEVNB]. Moreover, values determined by IFT are also given in Table 2.

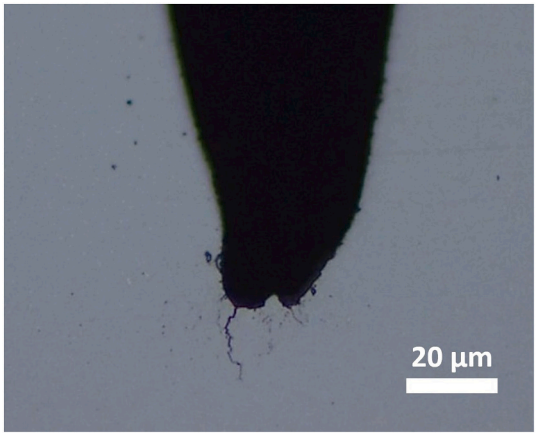

Fig. 4. Optical microscopy image showing notch aspect of a precracked SENB specimen.

Fracture toughness values reported have been determined after measurement, through fractographic inspection, of the effective length of notches and cracks before unstable failure takes place. Examples of fracture surfaces and distinct regions evidenced are given in **Figs. 6** and **7**, for representative SEμVNB and SENB-Cracked specimens. Very interesting, it is evidenced that in both cases, sudden failure took place from regions far from the geometrically defined notch, i.e. the one shaped by removal of material by either laser ablation or direct abrasive machining respectively. This was completely expected in the case of SENB-Cracked specimens, as fissures had been directly observed in the polished lateral sides of specimens before final testing (e.g. Fig. 5a). However, it was somehow uncertain for SEμVNB specimens, as there was not any direct information on through-thickness and depth characteristics of surface damage observed in the lateral faces just ahead of the laser-shaped notch tip (e.g. Fig. 2). This finding is indeed a necessary condition for validation of the use of SEμVNB specimens for measuring fracture toughness of cemented carbides, as it allows to conclude that small (but not negligible) and somehow controlled damage ahead of notch tip translates into effective precracking in these samples. Documentation and analysis of micromechanisms responsible for this damage-cracking evolution under applied load were out of the scope of this study, but they are subject of ongoing research and will be reported in future publications.

Low magnification FESEM micrographs were also useful for assessing and validating the existence of a uniform crack front through the whole thickness of the samples tested. In this regard, it should be stated that SEμVNB samples exhibit a notch/crack front more intrincate than SENB-Cracked ones, although variations are rather of small length scale (i.e. lower than 5 μm), and uniform along the whole thickness of the samples (Fig. 6). Effective length of existing cracks before sudden failure was determined by image contrast between distinct regions (e.g. Figs. 6 and 7) as well as specific fracture micromechanisms linked to changes induced by laser ablation, stable (under fatigue) and unstable extension of the crack. The latter are clearly described in the higher magnification FESEM micrographs shown in Figs. 8-10.

Direct and indirect effects of laser-matter interaction within SEμVNB samples may be discerned in Fig. 8. The former is related to effective material removal, i.e. geometrical notch (Fig. 8a), whereas the latter is a direct consequence of discontinuous small-scale damage - possibly as series of connected microcracks - induced just ahead of the notch tip (Fig. 8b). Direct transition from previously cracked region into unstable failure is clearly defined by the ductile dimples observed within the metallic binder in the lower part of Fig. 8c. These are well-established failure micromechanisms for cemented carbides, and are associated with the nucleation, growth and coalescence of microcavities formed when stretching the metallic enclaves as the existing cracks propagate in an unstable manner [41–44].

For the case of SENB-Cracked specimens, as it is seen in Fig. 9, it does not exist a clear topographic contrast between regions of stable and unstable crack growth; thus, definition of transition between them is rather based on detailed inspection of failure micromechanisms within the binder phase. Subcritical crack extension driven by cyclic loading is linked to step-like features localized within broken binder regions (Fig. 10a). This is completely different from the fractographic scenario defined by dimples within the metallic phase (as referred above), presented in a higher magnification in Fig. 10b, associated with unstable crack growth. As it has been reported by the authors in previous studies, absence of these ductile microcavities in fatigue fracture surfaces is a direct consequence of the suppression of the conventional toughening mechanism of hardmetals, i.e. ductile ligament reinforcement, by cyclic loading effects. Indeed, this is key for explaining the possibility of attaining stable crack extension at applied stress intensity factor values lower than fracture toughness in these extrinsically-toughened materials [39,40,45,46].

Experimental results determined from tests involving SEμVNB and SENB-Cracked samples showed a quite satisfactory agreement. In this

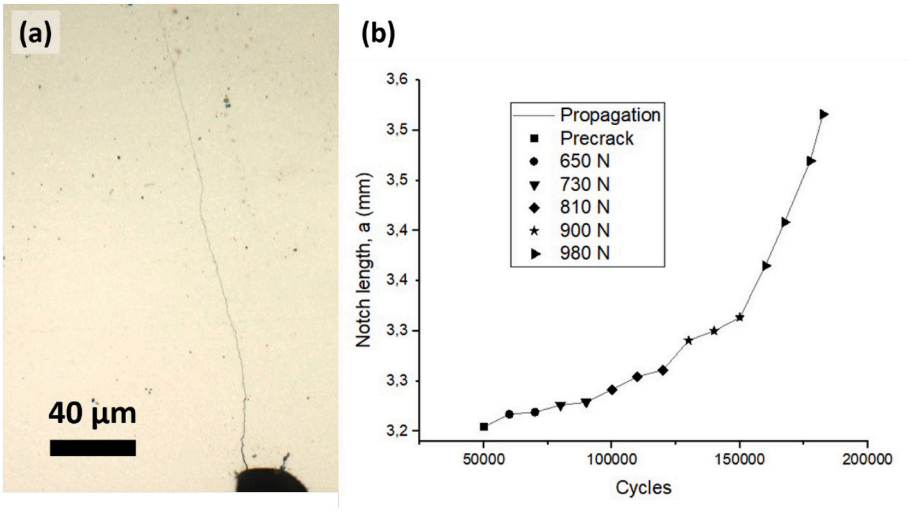

Fig. 5. (a) Optical microscopy image showing notch aspect of a SENB-Cracked specimen, after extension of initial precrack under tensile fatigue, and **(b)** corresponding crack extension behavior, as a function of number of cycles and maximum applied load under cyclic conditions ($R = 0.1$).

Table 2
Values of fracture toughness obtained, using different testing methods and sample geometries, for all hardmetal grades studied.

		Fracture toughness, MPa $m^{1/2}$			
		SEµVNB	SENB-Cracked	SEVNB*	IFT
Grade	U10	8.8 ± 0.5	9.5 ± 0.7	17.7 (35) 23.1 (42)	9.6 ± 0.3
	U20	9.7 ± 0.4	10.5 ± 0.5	16.3 (32) 18.4 (50)	10.9 ± 0.3
	U25	9.7 ± 0.8	10.9 ± 0.6	25.3 (39) 27.2 (74)	13.2 ± 0.3

* Corresponding radius of curvature (in microns) of induced V-notches placed into parenthesis.

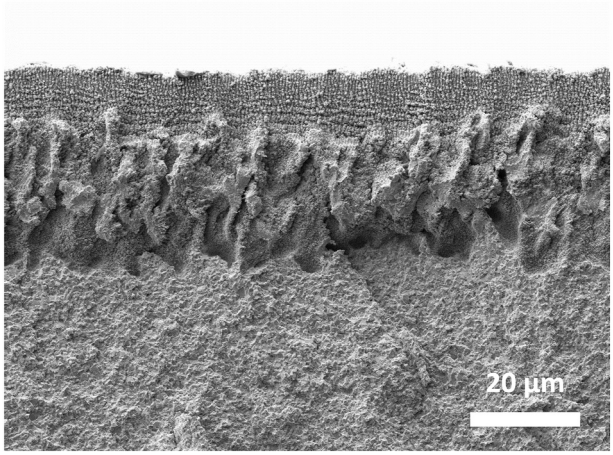

Fig. 6. Low magnification FESEM micrograph showing general fractographic scenario for a broken SEµVNB specimen.

regard, implementation of a simple statistical *t*-test allowed to confirm – at the 5% level of significance – that mean values for fracture toughness measured through flexural testing of either SEµVNB or SENB-Cracked specimens are "the same" in the case of U10 and U20 grades. However, similar analysis showed that they are "different" for U25 grade, fracture toughness in this case being slightly underestimated (by about 11%) when using SEµVN samples. Reasons for such small discrepancy for the grade with the highest binder content are not clear at this stage.

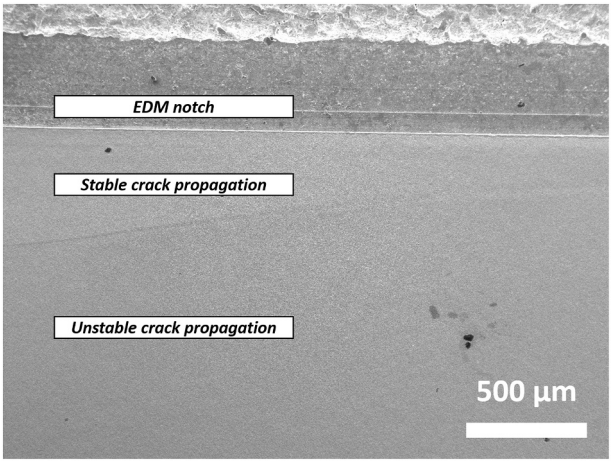

Fig. 7. FESEM micrograph showing general fractographic scenario for a broken SENB-Cracked specimen.

They are speculated to come from the existence of local (although always very small) residual stresses at the tip of the precrack or differences in the effective toughening developed just before unstable propagation of the previously introduced fissure. The former would point out a possible correlation between residual stresses during laser ablation and microstructure, as discussed below and a subject that may deserve further research efforts. The found agreement is further supported, within the limited conditions here studied, by the fact that dependence of fracture toughness upon microstructure follows well-established trends: grades with higher binder content exhibit higher fracture toughness (and lower hardness) values. Hence, as results measured using SENB-Cracked samples are considered in this study as baseline (reference) values for comparison purposes, these findings would allow to propose and validate flexural testing of SEµVNB specimens as an innovative and practical methodology for reliable determination of fracture toughness of cemented carbides. Existence of sharp, well-defined and residual-stress free cracks within SEµVNB samples is then implicit to above statement, and it is achieved as a direct result of the specific thermal and physical interaction between laser and matter when micronotching cemented carbides by means of UPLA, as it is now further discussed.

Ultrafast lasers provide extremely short, high intensity pulses which

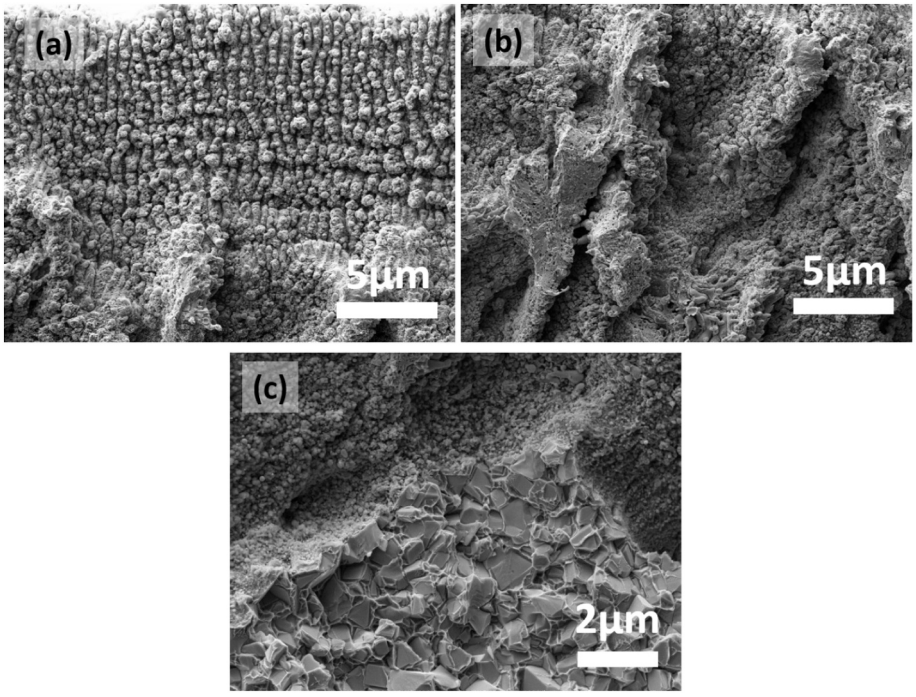

Fig. 8. FESEM micrographs showing specific failure micromechanism features existing in different regions evidenced at the surface of broken SEμVNB specimen given in Fig. 6: (a) geometrical notch resulting from effective removal of material by laser ablation; (b) "damaged/cracked" region just ahead of the physical notch; and (c) higher magnification image of previous micrograph highlighting borderline between the referred zone and the unstable failure one.

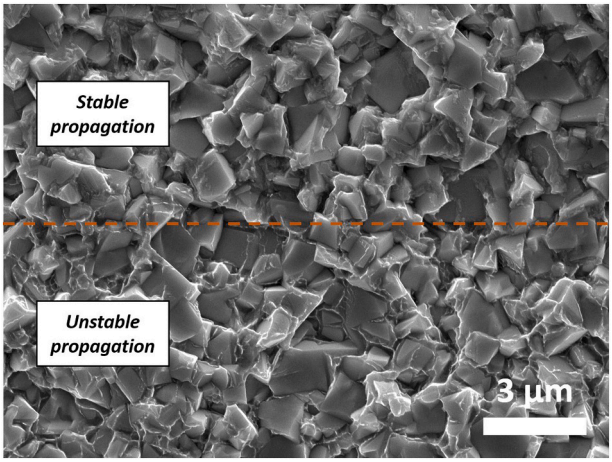

Fig. 9. FESEM micrograph showing transition between stable (linked to fatigue) and unstable failure regions at the surface of a broken SENB-Cracked specimen.

cause nonlinear photoionization and subsequent avalanche ionization. This leads to the generation of a free-electron plasma in dielectrics whose density, above a material-dependent threshold, yields to Coulomb explosion of a surface layer; and thus, non thermal ablation. Moreover, another mechanism coexists and easily overcomes the aforementioned one, as long as the pulse intensity exceeds the minimum value to induce ablation. In this case, very high transient temperatures in the electronic subsystem are induced as a result of light absorption by the electronic plasma, which reradiates towards the material surface and unleash a sudden non-adiabatic phase explosion. Notwithstanding the thermal nature of this ultrafast mechanism, the energy transferred to the remaining material is expected to be negligible since the ablated material is ejected in times less than some picoseconds, precluding significant thermal coupling to the substrate. Thus, regardless the ablation mechanism, the main advantage of ultrafast lasers, as compared with other micromachining techniques, is that material removal is linked to faint thermal collateral effects on the substrates.

Meanwhile, although ablation only takes place in the region where the beam has been tightly focused, the surrounding material may be affected by the shock waves generated in the ablation region. These shock waves can induce permanent microstructural modifications that can result in some stress of the material and subsequent microcracking in front of the notch tip along the propagation direction of the laser beam [36], as it was indicated previously. Furthermore, regarding residual stress state and magnitude, it has been reported that induced stresses are more than one order of magnitude smaller than those generated by other techniques (e.g. nanosecond laser ablation), and fall to zero typically in some tens of microns. Hence, all above scenario should effectively translate into the existence of a sharp, defined and residual-stress free crack-like feature ahead of the micronotch tip. This would sustain accuracy (U10 and U20 grades) and reliability of fracture toughness values measured by flexure testing of SEμVNB specimens. Nevertheless, the slight discrepancy measured for U25 grade highlights that further implementation of this fracture toughness testing methodology may require a deeper study on the correlation among laser ablation effects and microstructural assemblage of hardmetals, as a function of operating parameters, as energy-related issues could yield microstructural changes and/or stress states of quite different magnitudes. During laser fabrication processes, energy is focused on small spot sizes; thus, non-uniform heating/cooling of the material, leading to thermal contraction and expansion in response to the local thermal cycle, may take place. This is particularly important for composite materials where either above phenomena may be affected by relative differences of coefficient of thermal expansion among constitutive phases or phase transformations could take place as a consequence of laser processing, as it is the case of hardmetals (e.g. Ref. [21]).

Regarding the fracture toughness values measured using conventional SEVNB samples, they are overwhelmingly above the reference ones for the three materials studied. The main difference between (non-precracked) SEVNB and SENB-Cracked resides in the "effective existence

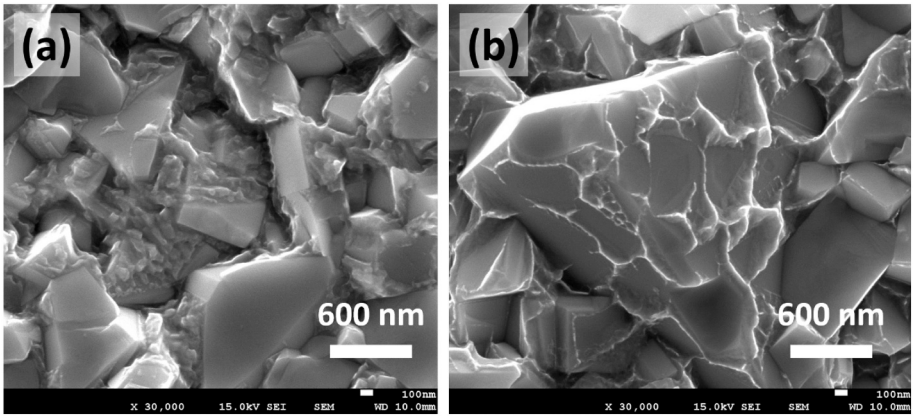

Fig. 10. FESEM micrographs of failure micromechanisms of metallic binder evidenced under (a) stable and (b) unstable crack extension: crystallographic step-like features and ductile dimples, respectively.

of a crack" in the case of the latter. Within this context, it may be concluded that width of notch tip, although achieving quite low values after diamond-polish sharpening, is not small enough for simulating the cracking-like scenario attempted. In this regard, notch widths are observed to be much higher than the 2–3 times factor empirically required, with respect to the microstructural length scale of the material (about 1 μm for the fine-grained hardmetals here studied) [11,12,47,48]; thus, notch is indeed acting as a geometrical stress concentrator but not as a real crack for which an appropriated stress intensity factor may be ascribed. Notch radius and crack-growth resistance behavior, i.e. extrinsic and intrinsic factors, could be recalled for reconciliation of the overestimated (apparent) fracture toughness values with those determined with the reference method, i.e. using SENB-Cracked samples (e.g. Ref. [12]). However, such analysis was out of the scope of this work because emphasis here was placed on the effective crack-like consideration of the existing notch. Nevertheless, it should be noticed that higher apparent fracture toughness values were measured for samples with higher notch radius, an experimental fact that sustains the feasibility of this analysis. Within this context, it may be considered as an alternative option for fracture toughness assessment, to be approached in future work.

Finally, and as expected, agreement between fracture toughness values measured by the IFT protocol and those determined using SEμVNB and SENB-Cracked samples is limited to the two hardest hardmetal grades under consideration. As it is well-established, as binder content or carbide grain size rises, the sharp-indentation mechanical response of cemented carbides starts to depart from the brittle-like nature required for reliable application of indentation fracture mechanics [13,16].

4. Conclusions

Fracture toughness of three microstructurally different WC-Co cemented carbides has been assessed using different testing methods and specimen geometries, the latter in terms of notch/crack configurations. Based on the obtained results the following conclusions may be drawn:

(1) Flexural testing of SEμVNB specimens, i.e. beams containing a shallow and through-thickness micronotch produced by UPLA, is proposed and validated as a reliable method for evaluation of fracture toughness of cemented carbides. This statement is sustained by the satisfactory agreement found between experimental values determined using this method and those measured employing previously cracked single-edge notched beams (SENB-Cracked), considered as baseline (reference) in this study.

(2) Suitability of SEμVNB method is linked to the effectiveness of UPLA for introducing sharp, defined and residual-stress free crack-like features ahead of a micronotch. This is possible because the extremely short interacion time of laser pulses with matter which yield small (although not negligible) and somehow controlled damage in front of the notch tip, as a result of shock wave propagation during ablation, together with faint (although possibly dependent on microstructure) thermal collateral effects on the remaining material.

(3) Comparison of fracture toughness values measured using SENB-Cracked and SEμVNB specimens with those determined by using simpler and more practical testing methods, such as flexural testing of SEVNB samples or indentation microfracture, indicates that feasibility of the latter is limited by partial unfulfillment of fracture mechanics requirements. In the case of SEVNB method, introduced V-notches were not sharp enough, as compared to microstructural length scale, to simulate an effective crack at the notch tip. Meanwhile, indentation-induced crack system was not well-defined for the lowest hardness cemented carbide studied; thus, assumptions invoked for applying indentation fracture mechanics were not satisfied. As a consequence, overestimated fracture toughness values were determined under these conditions.

Declaration of Competing Interest

The authors declare that they have no known competing financial interests or personal relationships that could have appeared to influence the work reported in this paper.

Data availability

The data that has been used is confidential.

Acknowledgements

The research work was conducted within a cooperative effort between Xiamen Tungsten Co., Ltd. and Universitat Politècnica de Catalunya. J.P-R. and P.M. acknowledge specific support from Junta de Castilla y León (Project SA136P20) and Ministerio de Ciencia e Innovación (PID2020-119003GB-I00) for UPLA activities conducted at Universidad de Salamanca. J.P.-R. also acknowledges support from Ministerio de Universidades (grant FPU17/01859).

References

[1] H.M. Ortner, P. Ettmayer, H. Kolaska, I. Smid, The history of the technological progress of hardmetals, Int. J. Refract. Met. Hard Mater. 49 (2015) 3–8, https://doi.org/10.1016/j.ijrmhm.2014.04.016.

[2] L. Prakash, Fundamentals and general applications of hardmetals, in: V.K. Sarin, D. Mari, L. Llanes (Eds.), Comprehensive Hard Materials, Volume 1 – Hardmetals, Elsevier, Oxford (UK), 2014, pp. 29–90, https://doi.org/10.1016/B978-0-08-096527-7.00002-7.

[3] B. Roebuck, E.A. Almond, Deformation and fracture processes and the physical metallurgy of WC–Co hardmetals, Int. Mater. Rev. 33 (1988) 90–112, https://doi.org/10.1179/imr.1988.33.1.90.

[4] B. Roebuck, M.G. Gee, R. Morrell, Developments in testing and mechanical properties of hard materials, Powder Metall. 39 (1996) 213–218, https://doi.org/10.1179/pom.1996.39.3.213.

[5] P. Kenny, The application of fracture mechanics to cemented carbides, Powder Metall. 14 (1971) 22–38, https://doi.org/10.1179/pom.1971.14.27.002.

[6] S. Suresh, The failure of hard materials in cyclic compression: theory, experiments and applications, Mater. Sci. Eng. A105 (106) (1988) 323–329, https://doi.org/10.1016/0025-5416(88)90713-6.

[7] E. Almond, B. Roebuck, Precracking of fracture-toughness specimens of hardmetals by wedge indentation, Met. Technol. 5 (1978) 92–99, https://doi.org/10.1179/mt.1978.5.1.92.

[8] R. Godse, J. Gurland, S. Suresh, Effects of residual stresses in fracture toughness testing of hard metals, Mater. Sci. Eng. A105 (106) (1988) 383–387, https://doi.org/10.1016/0025-5416(88)90721-5.

[9] M.N. James, A.M. Human, S. Luyckx, Fracture toughness testing of hardmetals using compression-compression precracking, J. Mater. Sci. 25 (1990) 4810–4814, https://doi.org/10.1007/bf01129946.

[10] Y. Yanaba, K. Hayashi, Relation between fracture surface area of a flexural strength specimen and fracture toughness for WC-10$_{mass}$%Co cemented carbide and Si_3N_4 ceramics, Mater. Sci. Eng. A209 (1996) 169–174, https://doi.org/10.1016/0921-5093(95)10123-3.

[11] Y. Torres, D. Casellas, M. Anglada, L. Llanes, Fracture toughness evaluation of hardmetals: influence of testing procedure, Int. J. Refract. Met. Hard Mater. 19 (2001) 27–34, https://doi.org/10.1016/S0263-4368(00)00044-5.

[12] Y. Torres, R. Bermejo, L. Llanes, M. Anglada, Influence of notch radius and R-curve behaviour on the fracture toughness evaluation of WC–Co carbides, Eng. Fract. Mech. 75 (2008) 4422–4430, https://doi.org/10.1016/j.engfracmech.2008.04.017.

[13] S. Sheikh, R. M'Saoubi, P. Flasar, M. Schwind, T. Persson, J. Yang, L. Llanes, Fracture toughness of cemented carbides: testing method and microstructural effects, Int. J. Refract. Met. Hard Mater. 49 (2015) 153–160, https://doi.org/10.1016/j.ijrmhm.2014.08.018.

[14] E. Chicardi, R. Bermejo, F.J. Gotor, L. Llanes, Y. Torres, Influence of temperature on the biaxial strength of cemented carbides with different microstructures, Int. J. Refract. Met. Hard Mater. 71 (2018) 82–91, https://doi.org/10.1016/j.ijrmhm.2017.11.003.

[15] A. Chychko, J. García, V. Collado Ciprés, E. Holmström, A. Blomqvist, HV-K_{Ic} property charts of cemented carbides: a comprehensive data collection, Int. J. Refract. Met. Hard Mater. 103 (2022) 105763, https://doi.org/10.1016/j.ijrmhm.2021.105763.

[16] D.K. Shetty, I.G. Wright, P.N. Mincer, A.H. Clauer, Indentation fracture of WC-Co cermets, J. Mater. Sci. 20 (1985) 1873–1882, https://doi.org/10.1007/BF00555296.

[17] J. Gurland, New scientific approaches to development of tool materials, Int. Mater. Rev. 33 (1988) 151–166, https://doi.org/10.1179/imr.1988.33.1.151.

[18] G. Dumitru, V. Romano, H.P. Weber, M. Sentis, W. Marine, Ablation of carbide materials with femtosecond pulses, Appl. Surf. Sci. 205 (2003) 80–85, https://doi.org/10.1016/S0169-4332(02)00906-6.

[19] G. Dumitru, B. Lüscher, M. Krack, S. Bruneau, J. Hermann, Y. Gerbig, Laser processing of hardmetals: physical basics and applications, Int. J. Refract. Met. Hard Mater. 23 (2005) 278–286, https://doi.org/10.1016/j.ijrmhm.2005.04.020.

[20] C. Karatas, B.S. Yilbas, A. Aleem, M. Ahsan, Laser treatment of cemented carbide cutting tool, J. Mater. Process. Technol. 183 (2007) 234–240, https://doi.org/10.1016/j.jmatprotec.2006.10.012.

[21] B. Denkena, B. Breidenstein, L. Wagner, M. Wollmann, M. Mhaede, Influence of shot peening and laser ablation on residual stress state and phase composition of cemented carbide cutting inserts, Int. J. Refract. Met. Hard Mater. 36 (2013) 85–89, https://doi.org/10.1016/j.ijrmhm.2012.07.005.

[22] S. Fang, L. Llanes, D. Bähre, Laser surface texturing of a WC-CoNi cemented carbide grade: surface topography design for honing application, Tribol. Int. 122 (2018) 236–245, https://doi.org/10.1016/j.triboint.2018.02.018.

[23] M. Hajri, P. Börner, K. Wegener, An industry-relevant method to determine material-specific parameters for ultra-short pulsed laser ablation of cemented carbide, Proc. CIRP 74 (2018) 709–713, https://doi.org/10.1016/j.procir.2018.08.036.

[24] S. Fang, D.W. Müller, C. Rauch, Y. Cao, F. Mücklich, L. Llanes, D. Bähre, Fabrication of interference textures on cemented carbides using nanosecond and femtosecond laser pulses, Proc. CIRP 87 (2020) 216–221, https://doi.org/10.1016/j.procir.2020.02.063.

[25] B. Denkena, A. Krödel, L. Ellersiek, M. Murrenhoff, Production of chip breakers on cemented carbide tools using laser ablation, Proc. CIRP 94 (2020) 834–839, https://doi.org/10.1016/j.procir.2020.09.114.

[26] S. Fang, S. Klein, D. Bähre, L. Llanes, Performance of laser surface textured cemented carbide tools during abrasive machining: coating effects, surface integrity assessment and wear characterization, CIRP J. Manuf. Sci. Technol. 31 (2020) 130–139, https://doi.org/10.1016/j.cirpj.2020.10.006.

[27] M. Zimmermann, B. Kirsch, Y. Kang, T. Herrmann, J.C. Aurich, Influence of the laser parameters on the cutting edge preparation and the performance of cemented carbide indexable inserts, J. Manuf. Process. 58 (2020) 845–856, https://doi.org/10.1016/j.jmapro.2020.09.003.

[28] H. Büttner, K. Michael, J. Gysel, P. Gugger, S. Saurenmann, G. de Bortoli, J. Stirnimann, K. Wegener, Innovative micro-tool manufacturing using ultra-short pulse laser ablation, J. Mater. Process. Technol. 285 (2020), 116766, https://doi.org/10.1016/j.jmatprotec.2020.116766.

[29] K.E. Hazzan, M. Pacella, T.L. See, Laser processing of hard and ultra-hard materials for micro-machining and surface engineering applications, Micromachines 12 (2021) 895, https://doi.org/10.3390/mi12080895.

[30] M.D. Shirk, P.A. Molian, A review of ultrashort pulsed laser ablation of materials, J. Laser Appl. 10 (1998) 18–28, https://doi.org/10.2351/1.521827.

[31] D. Bäuerle, Laser Processing and Chemistry, Springer-Verlag, Berlin Heidelberg, 2000, https://doi.org/10.1007/978-3-662-04074-4.

[32] J. Cheng, C.-S. Liu, S. Shang, D. Liu, W. Perrie, G. Dearden, K. Watkins, A review of ultrafast laser materials micromachining, Opt. Laser Technol. 46 (2013) 88–102, https://doi.org/10.1016/j.optlastec.2012.06.037.

[33] M. Turon-Vinas, M. Anglada, Fracture toughness of zirconia from a shallow notch produced by ultra-short pulsed laser ablation, J. Eur. Ceram. Soc. 34 (2014) 3865–3870, https://doi.org/10.1016/j.jeurceramsoc.2014.05.009.

[34] M. Turon-Vinas, M. Anglada, Assessment in Si_3N_4 of a new method for determining the fracture toughness from a surface notch micro-machined by ultra-short pulsed laser ablation, J. Eur. Ceram. Soc. 35 (2015) 1737–1741, https://doi.org/10.1016/j.jeurceramsoc.2014.12.024.

[35] L. Melk, M. Turon-Vinas, J.J. Roa, M.-L. Antti, M. Anglada, The influence of unshielded small cracks in the fracture toughness of yttria and of ceria stabilised zirconia, J. Eur. Ceram. Soc. 36 (2016) 147–153, https://doi.org/10.1016/j.jeurceramsoc.2015.09.017.

[36] M. Turon-Vinas, J. Morillas, P. Moreno, M. Anglada, Evaluation of damage in front of starting notches induced by ultra-short pulsed laser ablation for the determination of fracture toughness in zirconia, J. Eur. Ceram. Soc. 37 (2017) 5127–5131, https://doi.org/10.1016/j.jeurceramsoc.2017.07.006.

[37] D. Munz, T. Fett, Ceramics: Mechanical Properties, Failure Behaviour, Materials Selection, Springer-Verlag, Berlin Heidelberg, 1999, https://doi.org/10.1007/978-3-642-58407-7.

[38] H. Iizuka, M. Tanaka, Fracture toughness measurement with fatigue-precracked single edge-notched beam specimens of WC-Co hard metal, J. Mater. Sci. 26 (1991) 4394–4398, https://doi.org/10.1007/BF00543657.

[39] Y. Torres, J.M. Tarrago, D. Coureaux, E. Tarrés, B. Roebuck, P. Chan, M. James, B. Liang, M. Tillman, R.K. Viswanadham, K.P. Mingard, A. Mestra, L. Llanes, Fracture and fatigue of rock bit cemented carbides: mechanics and mechanisms of crack growth resistance under monotonic and cyclic loading, Int. J. Refract. Met. Hard Mater. 45 (2014) 179–188, https://doi.org/10.1016/j.ijrmhm.2014.04.010.

[40] J.M. Tarragó, J.J. Roa, V. Valle, J.M. Marshall, L. Llanes, Fracture and fatigue behavior of WC–Co and WC–CoNi cemented carbides, Int. J. Refract. Met. Hard Mater. 49 (2015) 184–191, https://doi.org/10.1016/j.ijrmhm.2014.07.027.

[41] L.S. Sigl, H.E. Exner, Experimental study of the mechanics of fracture in WC–Co alloys, Metall. Trans. A. 18A (1987) 1299–1308, https://doi.org/10.1007/BF02647199.

[42] L.S. Sigl, H.F. Fischmeister, On the fracture toughness of cemented carbides, Acta Metall. 36 (1988) 887–897, https://doi.org/10.1016/0001-6160(88)90143-5.

[43] J.M. Tarragó, E. Jiménez-Piqué, L. Schneider, D. Casellas, Y. Torres, L. Llanes, FIB/FESEM experimental and analytical assessment of R-curve behavior of WC–Co cemented carbides, Mater. Sci. Eng. A645 (2015) 142–149, https://doi.org/10.1016/j.msea.2015.07.090.

[44] J.M. Tarragó, D. Coureaux, Y. Torres, D. Casellas, I. Al-Dawery, L. Schneider, L. Llanes, Microstructural effects on the R-curve behavior of WC-Co cemented carbides, Mater. Design 97 (2016) 492–501, https://doi.org/10.1016/j.matdes.2016.02.115.

[45] L. Llanes, Y. Torres, M. Anglada, On the fatigue crack growth behavior of WC–Co cemented carbides: kinetics description, microstructural effects and fatigue sensitivity, Acta Mater. 50 (2002) 2381–2393, https://doi.org/10.1016/S1359-6454(02)00071-X.

[46] J.M. Tarragó, C. Ferrari, B. Reig, D. Coureaux, L. Schneider, L. Llanes, Mechanics and mechanisms of fatigue in a WC–Ni hardmetal and a comparative study with respect to WC–Co hardmetals, Int. J. Fatigue 70 (2015) 252–257, https://doi.org/10.1016/j.ijfatigue.2014.09.011.

[47] D. Munz, R.T. Bubsey, J.L. Shannon Jr., Fracture toughness determination of Al_2O_3 using four-point-bend specimens with straight-through and chevron notches, J. Am. Ceram. Soc. 63 (1980) 300–305, https://doi.org/10.1111/j.1151-2916.1980.tb10725.x.

[48] J. Kübler, Fracture toughness of ceramics using the SEVNB method: preliminary results, Ceram. Eng. Sci. Proc. 18 (1997) 155–162, https://doi.org/10.1002/9780470294444.ch18.